# Binding of Oxidized and Reduced Cytochrome $c_2$ to Photosynthetic Reaction Centers: Plasmon-Waveguide Resonance Spectroscopy†

S. Devanathan, Z. Salamon, G. Tollin, J. Fitch, T. E. Meyer, and M. A. Cusanovich*

*Department of Biochemistry and Molecular Biophysics, University of Arizona, Tucson, Arizona 85721*

*Received August 20, 2004; Revised Manuscript Received October 11, 2004*

ABSTRACT: The dissociation constants for the binding of oxidized and reduced wild-type cytochrome $c_2$ from *Rhodobacter capsulatus* and the lysine 93 to proline mutant of cytochrome $c_2$ to photosynthetic reaction centers (*Rhodobacter sphaeroides*) has been measured to high precision using plasmon-waveguide resonance spectroscopy. For the studies reported, detergent-solubilized photosynthetic reaction center was exchanged into a phosphatidylcholine lipid bilayer to approximate the physiological environment. At physiologically relevant ionic strengths (∼100 mM), we found two binding sites for the reduced wild-type cytochrome ($K_D$ = 10 and 150 nM), with affinities that decrease with decreasing ionic strength (2−5-fold). These results implicate nonpolar interactions as an important factor in determining the dissociation constants. Taking advantage of the ability of plasmon-waveguide resonance spectroscopy to reslove the contribution of changes in mass and of structural anisotropy to cytochrome binding, we can demonstrate very different properties for the two binding sites. In contrast, the oxidized wild-type cytochrome only binds to a single site with a $K_D$ of 10 nM at high ionic strength, and this site has properties similar to the low-affinity site for binding the reduced cytochrome. The binding of oxidized cytochrome $c_2$ has a strong ionic strength response, with the affinity decreasing ∼30-fold in going from high to low ionic strength. The K93P mutant binds to a single site in both redox states, which is similar, in terms of mass and structural anisotropy, to the oxidized wild-type site, with the affinity of the mutant oxidized state being ∼30-fold weaker than that of the oxidized wild-type cytochrome at high ionic strength. Thus, reduced wild-type cytochrome can bind to both the high- and low-affinity sites, while the oxidized wild-type cytochrome and both redox states of the mutant cytochrome can only bind to the low-affinity site, possibly the consequence of the more stable structure of reduced wild-type cytochrome. In aggregate, the results are consistent with a model in which a transient conformational change in the region 88−102 in the cytochrome three-dimensional structure, the so-called hinge region, drives the dissociation of the oxidized cytochrome from the reaction center−cytochrome complex, facilitating turnover.

A characteristic of many small, soluble, class I *c*-type cytochromes, for example, mitochondrial cytochrome *c* (cyt *c*)[1] and its nearest bacterial homologue cytochrome $c_2$ (cyt $c_2$) is that they shuttle between membrane-bound donors and acceptors. Thus, the oxidized cyt binds with specificity to an electron donor (for example cytochrome $b/c_1$), it is reduced, and the product dissociates. The reduced cyt then binds to an electron acceptor (for example, mitochondrial cytochrome oxidase or photosynthetic reaction center), transfers an electron, dissociates, and then repeats the cycle. Much of the focus has been on the interaction of reduced cytochromes with cytochrome oxidase or photosynthetic reaction center (RC), where electron transfer kinetics and binding constants have been measured. In the case of cytochrome oxidase, binding is usually measured using steady-state kinetics, hence $K_m$ values, and from analysis of the transient kinetics in the case of RCs.

The kinetics of interaction of cyt $c_2$ with RC are complex, but resolvable. Following incubation of the reduced cyt with detergent-solubilized RC in the dark, two kinetic phases for cyt oxidation are observed following a pulse of laser light, which initially generates the oxidized reaction center bacteriochlorophyll dimer ($RC^+$) and reduced quinone acceptor. The faster phase ($k_{ET}$) is a first-order electron transfer from the reduced cyt to $RC^+$, and the amplitude of this phase, but not the rate constant, is dependent on the concentration of the added cytochrome, consistent with *bound* cyt reducing the $RC^+$. The second, slower phase of cyt oxidation is pseudo-first-order. The rate constant is proportional and the amplitude inversely proportional to the cyt concentration, consistent with a second-order process ($k_{on}$) in competition with the faster first-order process. The dissociation constant for the binding of reduced cyt to reduced (or dark-adapted) reaction center ($K_D$) can be determined from analysis of the

† This work was supported in part by NIH grants GM21277 to M.A.C. and T.E.M. and GM59630 to G.T. and Z.S.

* To whom correspondence should be addressed. Telephone: (520) 621 7533. Fax: (520) 621 6603. E-mail: cusanovi@u.arizona.edu.

[1] Abbreviations: cyt, cytochrome(s); EDTA, ethylenediaminetetraacetic acid; HEPES, 4-(2-hydroxyethyl)-1-piperazineethanesulfonic acid; K93P, lysine 93 to proline cytochrome $c_2$ mutation; LDAO, lauryldimethylamine *N*-oxide; PC, phosphatidylcholine; PWR, plasmon-waveguide resonance; *R.*, *Rhodobacter*; RC, reaction center (s); Tris, tris(hydroxymethyl)aminomethane.

10.1021/bi0481904 CCC: $27.50 
Published on Web 12/04/2004

fraction of the fast phase as a function of cyt concentration. The reactions can be described by eq 1

$$\begin{array}{c} c_2(Fe^{2+}) + RC \xleftrightarrow{K_A = 1/K_D} c_2(Fe^{2+})-RC \\ h\nu\downarrow \qquad\qquad\qquad\qquad h\nu\downarrow \end{array} \tag{1}$$

$$c_2(Fe^{2+}) + RC^+ \underset{k_{off}}{\overset{k_{on}}{\leftrightarrow}} c_2(Fe^{2+})\text{-}RC^+ \overset{k_{ET}}{\leftrightarrow} c_2(Fe^{3+})-RC$$

where $c_2(Fe^{2+})$ is reduced cyt $c_2$, and $c_2(Fe^{3+})$ is oxidized cyt $c_2$.

Typically, $k_{ET}$ is on the order of $10^6$ $s^{-1}$, $K_D = 0.2-1$ $\mu$M, and $k_{on} \sim 10^9$ $M^{-1}$ $s^{-1}$ at pH 7−8 and 10−20 mM ionic strength (*1*−*6*). Moreover, a number of studies have found at least two binding sites for cyt $c_2$ and/or horse cyt *c* with RCs (*3*, *4*, *7*, *8*). There is considerable variation in the rate constants, dissociation constant, and stoichiometry, depending on the species used (RC and cyt), the ionic strength, the detergent concentration and type, the phospholipids used to make vesicles, and the pH (see ref *9* for a review). Note that $K_D$ and the ratio of $k_{on}/k_{off}$ are not necessarily the same, since they involve the binding of reduced cyt $c_2$ to two different species (RC and $RC^+$). Moreover, there are two additional binding constants, those for the interaction of oxidized cytochrome with RC and $RC^+$, which could play a role in the overall turnover of cytochrome under the appropriate conditions.

In the earliest direct determination of $K_D$, Rosen et al. (*2*) measured the binding of *Rhodobacter sphaeroides* cyt $c_2$ to *R. sphaeroides* reaction centers by equilibrium dialysis at low ionic strength (10 mM Tris-Cl, pH 8) and obtained $K_D$ values of 1 and 1.5 $\mu$M for the reduced and oxidized cyt $c_2$ to RC, respectively. The binding constant for reduced cyt $c_2$ is consistent with that derived from kinetic measurements under similar conditions (for example, 0.3 $\mu$M in 10 mM HEPES, pH 7.5, ref *10*). The turnover rate of horse cyt *c* with *R. sphaeroides* $RC^+$ as a function of ionic strength, specific ions, viscosity, temperature, light intensity, pH, and cyt concentration has been investigated (*5*). It was concluded that both $k_{on}$ and $k_{off}$ (eq 1) were ionic strength dependent and that turnover was retarded at low ionic strength, becoming maximal at ∼40 mM NaCl and declining sharply at higher ionic strengths.

Gerencser et al. (*5*) proposed that, at low ionic strength, the turnover rate is limited by the dissociation rate of the oxidized cyt, which inhibits the binding of reduced cyt. At high ionic strength, the binding of reduced cyt ($k_{on}$) is significantly weakened, thus accounting for the lower turnover. This analysis requires that $k_{off}$ be ionic strength dependent, but it is not clear why this should be the case. In a model that is dominated by electrostatics, increasing ionic strength would strongly affect the rate constant of formation of a reactive complex, but once the transient complex is formed, dissociation rate constants do not need to have the same ionic strength dependence. There are extensive data establishing a major role for positively charged side chains on the cyt in the region of the exposed heme edge, which interact with negatively charged side chains on the RC in the region of Y162 (light chain), facilitating formation of a transient complex, that account for the ionic strength dependence of $k_{on}$ (eq 1) (*6*, *10*). However, recent studies with *R. sphaeroides* RCs and cyt $c_2$ establish that hydrophobic residues affect both binding and electron transfer (*11*). This is consistent with a model in which long-range electrostatic interactions are key for docking and thus critical in association of the RC and cyt, but van der Waals, hydrophobic interactions, and hydrogen bonding are dominant in the final positioning and strongly influence $k_{ET}$ and $K_D$ (eq 1).

Differential binding of substrate and product in enzyme reactions is well-known to facilitate product dissociation following reaction. This is not difficult to envision because the substrate and product molecules generally have substantially different properties. One mechanism by which product dissociation (oxidized cyt for our purposes) might be facilitated is by a change in conformation of the cyt. However, the three-dimensional structures of oxidized and reduced cyt *c* and $c_2$ show minimal differences (e.g. ref *12*). Nevertheless, the crystal structures of oxidized cyt show higher temperature factors than for the reduced ones (e.g. ref *13*) and the stability of the oxidized cyt is less than that of the reduced ones (e.g. ref *14*). Likewise, the NMR solution structures of oxidized cyt appear to be more flexible/dynamic than for the reduced redox state (e.g. refs *15*, *16*). Therefore, a case might be made for a dynamic conformational change. Indeed, a number of investigators have suggested that such conformational changes might facilitate differential binding of cyt *c* to their electron transfer donors and acceptors (*13*, *17*). Differential binding of the two cyt redox states, with a 3−5-fold preference for oxidized cyt, at low ionic strength, has been reported for the interaction of cyt *c* with RCs (*18*, *19*).

It is well-known that oxidized, but not reduced, cyt *c* and $c_2$ undergo dynamic motion at pH 7 localized at the exposed heme edge, where electron transfer occurs (*20*). This dynamic process results in the transient dissociation of the sixth ligand methionine (*21*), which results in the rapid interconversion (27−42 $s^{-1}$) of the ligated, closed form of cyt *c* and $c_2$ to a more open, high-spin form that does not have a sixth ligand. This process has been studied through binding of exogenous ligands such as imidazole to the heme iron, where the conversion to the open form is required for imidazole binding (*22*). The three-dimensional structures of the imidazole complexes of horse cyt *c* and *R. sphaeroides* cyt $c_2$ indicate that 9−15 residues (termed the hinge) could be involved in the dynamic conformational change (*23*, *24*). We have been studying the dynamics of the hinge (sequence positions 88−102 in *Rhodobacter capsulatus* cyt $c_2$) through a combination of site-directed mutagenesis and measurement of equilibrium and kinetics of imidazole binding (*25*). Importantly, we have characterized cyt $c_2$ mutants that have markedly altered affinities for imidazole with up to 20-fold faster kinetics for hinge movement. Thus, if hinge movement plays a role in the dissociation of the oxidized protein from RCs, mutants with altered kinetics may affect the apparent $K_D$, by altering $k_{off}$ (eq 1). This provides a mechanism for differential binding, which can be tested.

Surface plasmon resonance and its more recent variant, plasmon-waveguide resonance (PWR), provide a means to accurately measure binding of ligands to membrane receptors (*26*). Thus, using PWR, we can directly measure the binding of both cyt $c_2$ (wild-type and mutants) redox states to RC incorporated into lipid bilayers. Importantly, PWR can also

characterize conformational changes that accompany such binding (*27*, *28*). We will show here that differential binding of cyt $c_2$ redox states to RCs occurs under the appropriate solution conditions and that binding of the oxidized but not the reduced protein is markedly altered when a mutant that affects hinge dynamics is used.

## MATERIALS AND METHODS

*Purification of Photosynthetic RCs and Cyt $c_2$.* Cyt $c_2$, the cyt $c_2$ mutant K93P, and *R. sphaeroides* RCs were prepared as previously described (*10*, *25*). Guanidine-HCl denaturation, redox potentials, and the alkaline p$K_a$ monitored by the loss of the 695 nm band were determined as previously described (*20*). All PWR studies were carried out in 10 mM Tris-Cl, pH 7.3, supplemented with either 10 or 100 mM KCl to yield ionic strengths of 19 or 109 mM, respectively, at ambient temperature.

*PWR Spectroscopy*. PWR spectroscopy is based upon the resonant excitation by polarized light from a CW He−Ne laser of surface plasmons in a thin metal film (Ag) deposited on the surface of a glass prism under total internal reflection conditions. Plasmon excitation is coupled with the excitation of waveguide modes due to an overcoating of a dielectric layer ($SiO_2$) on the silver film. Plasmon formation generates an evanescent electromagnetic field localized at the outer surface of the PWR sensor that decays exponentially with increasing distance from the metal−dielectric interface (*26*). Resonance is achieved by varying the incident angle ($\alpha$) at a fixed wavelength ($\lambda$). The intensity of the reflected light is diminished due to plasmon excitation that occurs at the expense of the incident light energy. A plot of reflected light intensity vs incident angle constitutes a PWR spectrum.

Resonances can be excited with light whose electric vector is polarized either perpendicular (*p*) or parallel (*s*) to the resonator surface and can be used to probe the properties (refractive index, *n*; extinction coefficient at the excitation wavelength, *k*; and thickness, *t*) of a layer of molecules immobilized on the silica surface (*29*). This allows the characterization of uniaxially ordered anisotropic systems such as proteolipid membranes that are deposited on the resonator surface, as well as changes in mass density and conformation occurring as a consequence of biomolecular interactions. The PWR spectrum can be described by the depth, the half-width, and the angular position of the resonances, which are determined by the optical characteristics of the sensor and the immobilized molecules. Molecular interactions occurring at the surface are detected as changes in these spectral characteristics. Thus PWR provides a means to directly measure the binding of oxidized and reduced cytochromes to RCs incorporated in a lipid bilayer.

*Insertion of Reaction Centers into Solid-Supported Lipid Bilayer*. Self-assembled solid-supported lipid bilayers were used in the present experiments (*30*). The lipid membrane was formed using a solution of 8 mg/mL egg phosphatidylcholine (egg PC; Avanti Polar Lipids, Birmingham, AL) in butanol/squalene (0.93/0.07, v/v). Phosphatidylcholine is an important component of the *R. sphaeroides* chromatophore membrane (23−32% of total lipid P, depending on strain) along with phosphatidylethanolamine (25−27%) and phosphatidylglycerol (37−39%) (*31*). The method for membrane preparation involves spreading a small amount of lipid solution across an orifice in a Teflon block separating the silica surface of the PWR resonator from the aqueous phase. The hydrated silica surface attracts the polar groups of the lipid molecules to form a monolayer with the hydrocarbon chains oriented toward the excess lipid solution. Spontaneous bilayer formation is initiated when the sample compartment of the resonator is filled with an aqueous solution, resulting in a thinning process to form the second monolayer of the lipid and a plateau−Gibbs border consisting of lipid solution that anchors the bilayer to the Teflon block. This border allows excess lipid solution to flow in or out of the orifice in response to protein insertion and/or conformational changes.

*R. sphaeroides* RC molecules were incorporated into such a preformed lipid bilayer by addition of 12.5 $\mu$L of an 80 $\mu$M solution of RC, solubilized in buffer containing 35 mM octyl glucoside, to the aqueous compartment of the PWR cell (volume 1 mL). This results in dilution of the detergent to below the critical micelle concentration (25 mM) and to spontaneous transfer of the protein from the detergent micelle into the lipid membrane. Typically, the bilayer was washed with the reaction buffer, although residual octyl glucoside did not appear to affect measured binding constants. It is not possible to measure the amount of RC incorporated into the bilayer, but to ensure bilayer flexibility, less than saturating amounts of RCs were added. It is not necessary to know the absolute RC concentration, since the PWR spectral shift is directly proportional to the amount of cyt bound, which is much smaller than the concentration of cyt added to the PWR cell. Note that RCs are incorporated in both directions. However, only those with interaction domains facing the aqueous volume will bind cyt (~50%). All PWR spectral measurements reported here have been obtained with a 543 nm laser light source using a Beta PWR instrument from Proterion Corp. (Piscataway, NJ) with an angular spectral resolution of 1 mdeg, and reproducibility was also ±1 mdeg.

*Graphical Analysis of PWR Spectra.* Analysis of PWR spectral data can be accomplished by either theoretical fitting using thin-film electromagnetic theory based on Maxwell's equations (*32*) or by a graphical analysis approach (*28*). To analyze the complex binding interactions between cyt $c_2$ and RC, we have used the graphical analysis approach to deconvolute the components of the PWR spectral shifts that are due to changes in structural anisotropy and in proteolipid mass, as reflected by the *p*- and *s*-polarized resonances. Changes in mass density are due to addition or subtraction of mass from the membrane (either protein or lipid or both), resulting in changes in refractive index and thickness. Changes in mass distribution result from structural changes (i.e., long-range molecular order and molecular conformations) occurring at the resonator surface, resulting in changes in refractive index anisotropy. Furthermore, although both mass density and anisotropy changes can result in changes of spectral position, the alteration of mass density results in isotropic changes of these properties (i.e., *s*-shifts equal in magnitude and direction to *p*-shifts), whereas alterations in structure cause anisotropic changes (i.e., *s*-shifts different in magnitude and direction from *p*-shifts). One can distinguish mass changes from structural changes by transforming spectral shift variations from an orthogonal (*s*−*p*) coordinate system into a (mass−structure) one. The procedure for doing

this is described by Salamon and Tollin (*28*). Once this has been accomplished, each point on the mass axis ($\Delta_m$) can be expressed by changes of the original coordinates ($\Delta s$ and $\Delta p$) as follows

$$\Delta_m = [(\Delta s)^2_m + (\Delta p)^2_m]^{1/2} \quad (2)$$

and on the structural axis

$$\Delta_{str} = [(\Delta s)^2_{str} + (\Delta p)^2_{str}]^{1/2} \quad (3)$$

In this way, the contribution of structural changes and mass alterations are expressed in terms of angular shifts.

In this work, the PWR sensor was experimentally calibrated by measuring the PWR spectra obtained from a bare resonator surface (i.e., without lipid bilayer and RC) in contact with aqueous buffer containing varying amounts of either KCl or KBr using *p*- and *s*-polarized light. The resulting spectral shifts were plotted as a function of salt concentration, and the slope was used to obtain the sensitivity factor ($S_f$). Similar results were obtained with both salts. With the present sensor, the *s*-polarized resonances had a greater mass sensitivity than *p*-polarized resonances, resulting in a sensitivity factor $S_f = \Delta s/\Delta p = 1.56 \pm 0.02$.

## RESULTS

*PWR Spectral Changes Occurring upon RC Incorporation.* The insertion of RCs into the phospholipid bilayer was followed by PWR spectra resulting from changes in mass density and molecular order, due to the formation of a proteolipid membrane that was spectrally different from the bilayer without the RC, as shown in Figure 1. The PWR spectra of the bilayer (dashed curves) show a large shift in resonance position toward higher angles of incidence (curves 1), as well as changes in spectral amplitude, for both *p*- and *s*-polarization. Insertion of the RC was anisotropic, i.e., *p*-shifts > *s*-shifts; note that these values correspond to actual experimental observations, without correction for the difference in sensitivity of the *s*- and *p*-resonances. This anisotropy is a consequence of the overall cylindrical shape of the RC and is evidence for a uniaxial insertion process with the long axis of the RC perpendicular to the membrane plane, resulting in an increase in the structural anisotropy of the bilayer.

*RC-Reduced Wild-Type Cyt $c_2$ Binding.* For the binding of cyt $c_2$ to RCs, we focused initially on a relatively high ionic strength (109 mM) to approximate physiological conditions. For the conditions under which we grow *R. sphaeroides*, the fresh growth media has an ionic strength of ~140 mM and the spent media is ~75 mM. The periplasmic space, where cyt $c_2$ interacts with the RC, should have an ionic strength similar to that of the growth medium. Moreover, egg PC was used to prepare the phospholipid bilayer, since PC is an important phospholipid component in both *R. sphaeroides* and *R. capsulatus* membranes (*31*, *33*). However, it is possible to make bilayers having mixed lipid compositions, and this might be of interest in future extensions of these studies. After incorporation of the RC into an egg PC bilayer in contact with a 10 mM Tris-Cl/100 mM KCl buffer, pH 7.3, aliquots of a solution of reduced *R. capsulatus* cyt $c_2$ in the same buffer (reduced with a small excess of dithionite just before the binding experiment) were added to the sample compartment in the dark. The binding of reduced cyt $c_2$ to RCs resulted in significant changes in the position, depth, and amplitude of the PWR spectrum (Figure 1A,B, curves 2 and 3). A biphasic binding process was observed. At low cyt $c_2$ concentrations (<0.1 $\mu$M), an anisotropic shift to lower angles was observed for both *p*- and *s*-polarization (curves 2, *p*-shifts > *s*-shifts), accompanied by a decrease in spectral amplitude. Further increases in cyt $c_2$ concentrations (>0.2 $\mu$M) resulted in an anisotropic spectral shift toward higher incident angles, with an increase in spectral amplitude (curves 3, *p*-shifts > *s*-shifts).

Plots of the resonance shifts for *p*- and *s*-polarized light as a function of added cyt $c_2$ are presented in Figure 2A. These biphasic curves were fit with two hyperbolic functions of opposite sign to obtain the deconvoluted curves labeled 1−4 (data points were not weighted during fitting). The solid lines through the data points correspond to the sum of curves 1 and 2 (curve 5, *p*-polarized resonance shifts) and curves 3 and 4 (curve 6, *s*-polarized resonance shifts). As is evident, these deconvoluted curves yield excellent fits to the data. The high- and low-affinity dissociation constants obtained from these deconvolutions are reported in Table 1. Control experiments, in which similar concentrations of cyt $c_2$ were added to a preformed bilayer in the absence of RC, did not result in spectral shifts (data not shown). This establishes that the observed changes result from binding interactions between the reduced cyt $c_2$ and the RC.

The relatively high ionic strength used in these experiments is not typical of kinetic studies of the cyt $c_2$−RC interaction using detergent-solubilized RCs, where relatively low ionic strength (10−20 mM) is typically used to enhance the electrostatic effects. Moreover, the apparent affinities reported here (Table 1) are higher than expected from the kinetic studies ($K_D$ = 300−700 nM). Thus for comparison, we have measured the dissociation constants for the interaction of reduced wild-type cyt $c_2$ and RCs at 19 mM ionic strength. Panels E and F of Figure 1 present typical PWR spectra for both *p*- and *s*-polarization, with the resulting plots of PWR shifts against cyt $c_2$ concentration shown in Figure 2B, along with the fitted curves, and corresponding affinities are summarized in Table 1. As with high ionic strength, we find two binding sites. These have lower affinities than found at high ionic strength and again appear to have a 1:1 stoichiometry. The low affinity site ($K_D$ = 270 nM) has a dissociation constant consistent with the kinetic studies. However, as the ionic strength is increased from 19 to 109 mM, the affinity increases, contrary to expectations based upon a purely electrostatic binding mechanism. This observation will be addressed in the Discussion. Note that the magnitude of the PWR shifts (in mdeg) is dependent on the amount of cyt bound and the magnitude of the resulting mass and structural changes (see below for graphical analysis).

*RC-Oxidized Wild-Type Cyt $c_2$ Binding.* The PWR spectral effects for oxidized cyt $c_2$ binding at 109 mM ionic strength are shown in Figure 1, panels C and D. These involve an anisotropic increase in amplitude for both *p*- and *s*-polarization, as well as a shift to higher incident angles that occurs at all cyt concentrations. This is quite different behavior than was observed with reduced cyt $c_2$, i.e., monophasic binding occurs as a function of increasing $c_2$ concentration (Figure 3A). The data could be fit with a single hyperbolic function, yielding a binding constant ($K_D$ = 10 nM) that is similar in

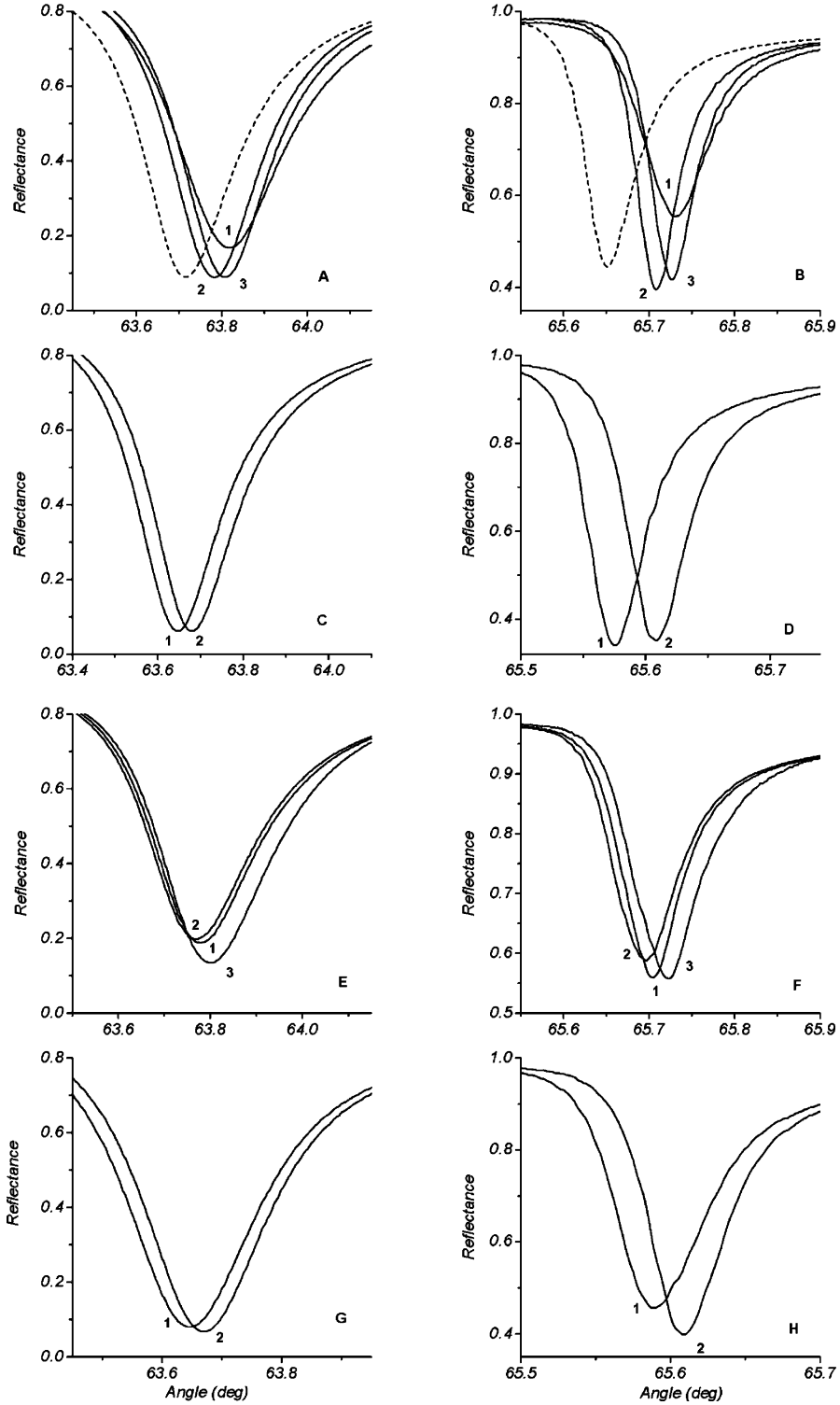


FIGURE 1: PWR spectra showing insertion of *R. sphaeroides* RC into egg PC bilayer and interaction of cyt $c_2$ with bilayer incorporated RC. (A, B) Reduced cyt $c_2$ ($I$ = 109 mM, pH = 7.3). PWR spectral changes for *p*-polarized (left panel) and *s*-polarized (right panel) light excitation obtained for solid-supported egg PC bilayer (dashed line), and after equilibration of incorporated RC (curve 1) in Tris-Cl/KCl buffer (see methods; final bulk concentration of RC in sample cell = 1 $\mu$M). PWR spectra obtained after making the solution 0.05 $\mu$M (curve 2) and 0.5 $\mu$M (curve 3) in reduced cyt $c_2$. (C, D) Oxidized cyt $c_2$ ($I$ = 109 mM, pH = 7.3). PWR spectra of RC inserted into an egg PC bilayer (curve 1) and after making the solution 0.25 $\mu$M in oxidized cyt $c_2$ (curve 2). (E, F) Reduced cyt $c_2$ ($I$ = 19 mM, pH = 7.3). PWR spectra of RC in egg PC bilayer (curve 1) and after making the solution 0.08 $\mu$M (curve 2) and 1.5 $\mu$M (curve 3) in reduced cyt $c_2$. (G, H) Oxidized cyt $c_2$ ($I$ = 19 mM, pH = 7.3). PWR spectra of RC incorporated into an egg PC bilayer (curve 1) and on making the solution 2.5 $\mu$M in oxidized cyt $c_2$ (curve 2).

form (positive PWR shift) to the second phase (low affinity) of the reduced cyt $c_2$ binding (Table 1) at this ionic strength, but with a $K_D$ like that of the high affinity site. Over the entire concentration range investigated here, the high-affinity binding, the left spectral shift process observed with the reduced cyt, is absent.

At low ionic strength (19 mM), oxidized cyt $c_2$ also binds monophasically at a single site (Figure 1, panels G and H),

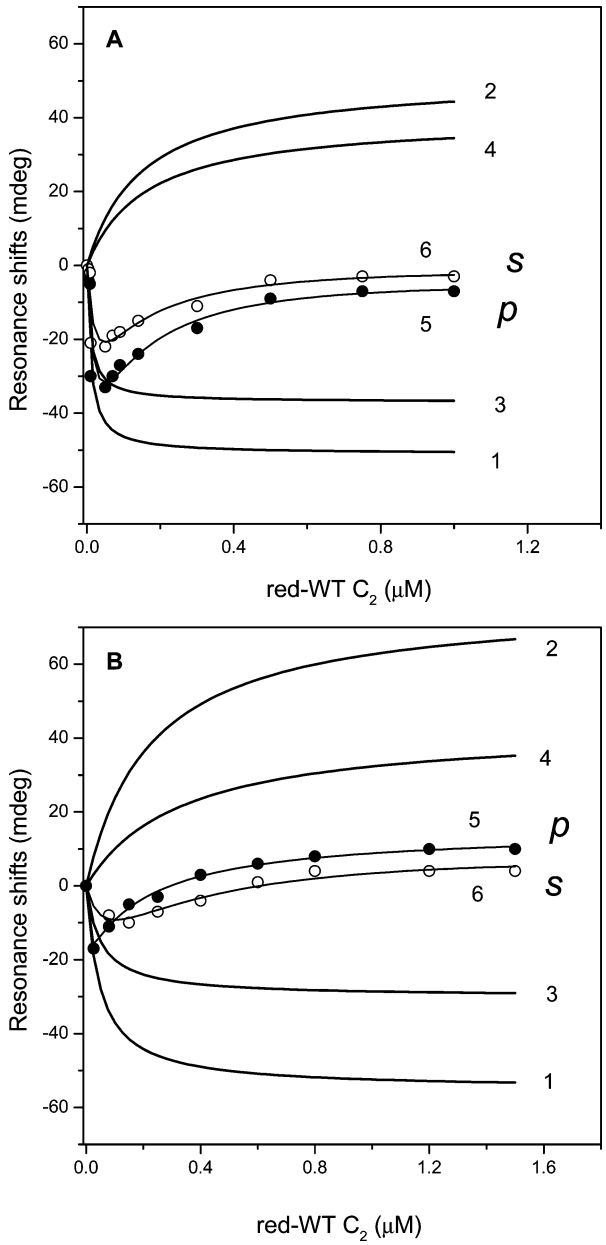


FIGURE 2: PWR spectral position minimum plotted as a function of the concentration of reduced cyt $c_2$. (A) Plots of PWR spectral shifts occurring upon addition of aliquots of reduced cyt $c_2$ to membrane-incorporated RC for *p*-polarization (closed symbols) and *s*-polarization (open symbols) at 109 mM ionic strength, pH 7.3. Negative values are indicative of resonance shifts to smaller incident angles. Hyperbolic deconvolutions of the experimental data are presented as curves 1−4 (dissociation constants given in Table 1) for both panels. Curve 5 is a summation of curves 1 and 2, and curve 6 is a summation of curves 3 and 4 for both panels. (B) Plots of PWR spectral shifts at 19 mM ionic strength, pH 7.3, with details as for panel A. The estimated error in resonance angle positions in this and other figures is ±1 mdeg.

with an affinity 33-fold lower than that at high ionic strength (Figure 3B and Table 1). Thus, as with the binding of reduced cyt $c_2$, the affinity for the oxidized cyt increases with an increase in ionic strength from 19 to 109 mM. Note that the affinity and positive PWR shift for oxidized cyt $c_2$ at low ionic strength is approximately that of the low-affinity site for the reduced cyt at this ionic strength.

*K93P Properties.* The K93P mutant was chosen for these studies as it has a much increased rate constant for the hinge

Table 1: $K_D$ Values for Cyt $c_2$−RC Interaction

| | $K_D$ (nM)[a] for different cytochrome redox states | |
|---|---|---|
| cytochrome | oxidized | reduced |
| | Ionic Strength = 109 mM | |
| wild-type | 10 ± 2 | 10 ± 1, 150 ± 2 |
| K93P | 310 ± 90[b] | 24 ± 2 |
| | Ionic Strength = 19 mM | |
| wild-type | 330 ± 30 | 54 ± 3, 270 ± 30 |
| K93P | 165 ± 35[b] | 48 ± 4 |

[a] $K_D$ values are the average of those determined from the *p*- and *s*-polarization fits. [b] Oxidized K93P titrations were fit with two hyperbolic curves, the major component (~80% of the total) yielded the $K_D$ reported, the minor component (~20%) was the $K_D$ of the reduced species (see the text).

movement in the oxidized form relative to the wild-type cyt, involving breakage of the Fe−methionyl sulfur bond and allowing the heme face to become available to exogenous ligands (*25*). Thus, this rate constant ($k_{12}$) increases from ~35 to ~700 $s^{-1}$ for the K93P mutant (*25*). The stability of oxidized K93P relative to oxidized wild-type cyt is decreased by ~1.6 kcal/mol based on guanidine-HCl titrations monitored by circular dichroism in the far UV. The p$K_a$ for the alkaline titration of the 695 nm band is 7.7 for oxidized K93P, compared to 9.6 for the wild-type cyt, consistent with a substantial weakening of the Fe−methionyl sulfur bond. The redox potential of K93P is 300 mV, suggesting that the reduced form is destabilized ~1.5 kcal/mol relative to the oxidized form. Thus, the net destabilization of reduced K93P as compared to wild-type is ~3 kcal/mol.

*RC−K93P Binding.* The interactions of the *R. capsulatus* cyt $c_2$ hinge mutant K93P with membrane-bound RC were investigated for both redox states. Plots of the resonance shifts for *p*- and *s*-polarized light as a function of added K93P are given in Figure 3C,D for oxidized and reduced species at high ionic strength. The $K_D$ values for the fits are summarized in Table 1. For the reduced mutant, the PWR shift occurred to larger angles at all concentrations (Figure 3D), completely eliminating the biphasic behavior observed with wild-type cyt $c_2$. Reduced K93P bound ~2-fold less tightly as reduced wild-type cyt (relative to the high-affinity site) but ~7-fold more tightly than the low-affinity site. The oxidized K93P data (both ionic strengths) were fit with two binding sites, ~80% was fit (Figure 3C) with the $K_D$ values reported in Table 1. The second phase (~20% of the curve) had a $K_D$ that within experimental error was that found for the reduced protein, as apparently the oxidized K93P autoreduced during the course of the experiment. The principal impact of this complication was an increased error in the $K_D$ values. The oxidized mutant bound 31-fold more weakly than oxidized wild-type cyt and 13-fold less tightly than reduced K93P. These results will be discussed further below.

The $K_D$ values for the binding of oxidized and reduced K93P at 19 mM ionic strength are given in Table 1 (data not shown). However, unlike the oxidized wild-type cyt, the affinity for oxidized K93P decreases with increasing ionic strength. In contrast, reduced K93P has an affinity that increases with increasing ionic strength, albeit only 2-fold, but similar to the wild-type cyt.

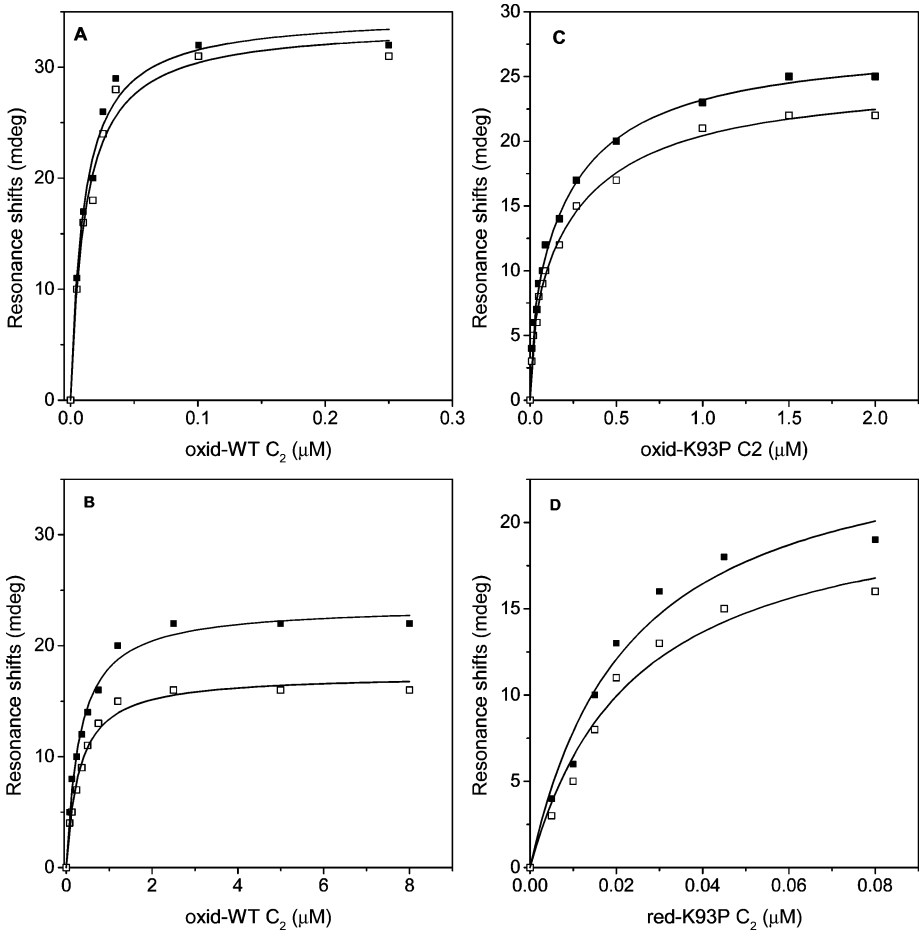


FIGURE 3: Plots of PWR resonance minima positions as a function of cyt concentration. Data for *p*-polarized (closed squares) and *s*-polarized spectral shifts (open squares) are presented. Solid lines show the fit to the experimental data by a single hyperbolic function; dissociation constants are reported in Table 1. (A) Oxidized cyt $c_2$, ionic strength = 109 mM. (B) Oxidized cyt $c_2$, ionic strength = 19 mM. (C) Oxidized K93P, ionic strength 109 mM. (D) Reduced K93P, ionic strength 109 mM.

*Graphical Data Analysis.* Figure 4 presents an (*s*−*p*)-coordinate plot of the high ionic strength data shown in Figures 2 and 3, containing both mass and structural axes placed according to the sensitivity of the PWR sensor (cf. Materials and Methods). The origin in this plot corresponds to the values obtained for the RC inserted into a lipid bilayer prior to addition of any cyt $c_2$. Thus, all of the data points shown refer to shifts induced by cyt binding. The deconvoluted *s*- and *p*-spectral shifts obtained for the biphasic reduced cyt $c_2$ binding to the RC and also the simple hyperbolic binding for oxidized cyt $c_2$ and the oxidized and reduced K93P mutant are shown. Note that the high-affinity process for the reduced cyt $c_2$ binding falls in the third quadrant of this plot (corresponding to negative values for both *p*- and *s*-shifts), whereas the lower affinity binding process for the reduced cyt, as well as all other data sets corresponding to oxidized cyt $c_2$ and to mutant cyt $c_2$ binding, fall within the first quadrant (corresponding to positive values for *p*- and *s*-shifts). Note also that the slopes of these plots all differ substantially, reflecting shifts to varying extents toward the mass and structural axes. Such differences in slope are the result of differences in the contributions of mass changes and structural anisotropy changes to the spectral shifts and thus allow values for the magnitudes of these changes to be obtained as a function of cyt $c_2$ concentration. These are shown in Figure 5 for reduced cyt $c_2$.

Figure 5 shows that the negative changes obtained for the high-affinity binding processes of the reduced wild-type cyt are a result of decreases in both the mass density and in the structural anisotropy of the proteolipid system and that the positive changes for the low-affinity binding processes are due to increases in both mass density and in structural anisotropy. Thus, this analysis allows one to distinguish the physical processes involved in these binding events. It is important to point out that a decrease in mass density in this situation, in which mass is clearly being added to the system by cyt binding to the membrane-bound RC, can only result from expulsion of lipid from the bilayer as a consequence of protein conformational changes. We will return to this point below. The same procedure was used to analyze the oxidized wild-type, oxidized K93P, and reduced K93P but with only a single hyperbolic curve.

Table 2 presents values for the percentage contributions to the total spectral shift of mass changes on binding, along with the ratio of the fraction mass change to fraction structural anisotropy change for both wild-type and K93P, their two redox states, and at two ionic strengths. It is clear that, for the wild-type cytochrome, binding of the reduced form results in a larger percentage of structural change, and therefore a smaller ratio, than is the case for the oxidized form. The difference between redox states is significantly

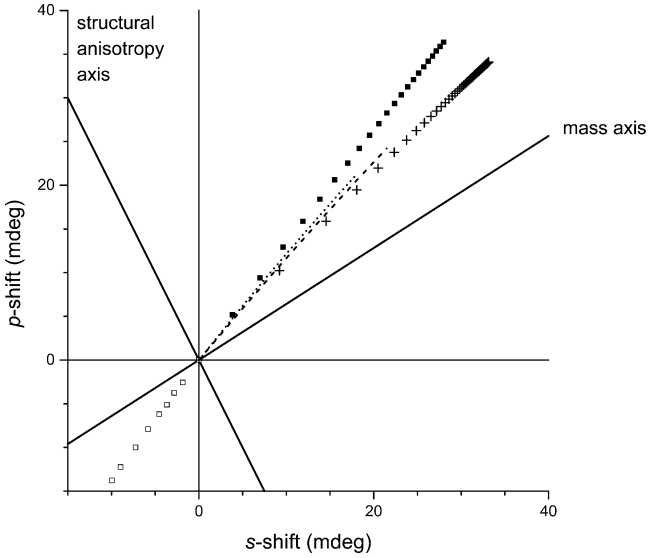


FIGURE 4: Plots of PWR spectral shifts on an ($s-p$) coordinate system containing mass and structural anisotropy axes for the binding of cyt $c_2$ to reaction center. Deconvoluted pairs of hyperbolic curves from Figure 2 for the binding of reduced wild-type cyt $c_2$ (109 mM ionic strength): □, high-affinity binding; ■, low-affinity binding. Hyperbolic curves from Figure 3A for binding of oxidized cyt $c_2$ (109 mM ionic strength, +), and hyperbolic curves from Figure 3C,D for binding of K93P mutant (oxidized, 109 mM ionic strength, dashed line; reduced, 109 mM ionic strength, dotted line).

smaller for the K93P mutant. A molecular interpretation of these changes will be presented below.

## DISCUSSION

Using PWR spectroscopy applied to RCs incorporated into a phospholipid bilayer, we have shown that $K_D$ values can be measured with high precision for cyt $c_2$ binding. A considerable amount of work has been done on the interaction of RCs with cyt as discussed in the Introduction, particularly cyt $c_2$, with the reaction scheme shown in eq 1 being generally applicable, but with considerable variation in the reported kinetic constants and stoichiometry depending on conditions (pH, ionic strength, detergent concentration, lipid composition, cyt source, etc). In the context of eq 1, $K_D$ is 270 nM for the low-affinity binding of reduced *R. capsulatus* cyt $c_2$ to *R. sphaeroides* RCs (Table 1) at 19 mM ionic strength, similar to that recently reported from kinetic analysis (500 nM) using the same proteins at a slightly lower ionic strength and with detergent-solubilized (0.04% dodecyl $\beta$-maltoside) RC (*10*). In this same study, the $K_D$ for the binding of reduced *R. sphaeroides* cyt $c_2$ to *R. sphaeroides* RCs was found to be 340 nM. However, a high-affinity site was not observed in the Tetreault et al. (*10*) study ($K_D = 54$ nM at 19 mM ionic strength). In contrast, a number of authors have reported at least two binding sites (or cyt conformations) (*3*, *4*, *7*, *8*) for the interaction of cyt and RCs. For example, Tiede et al. (*4*) reported that two first-order reactions ($\tau = 0.5$ and 3 $\mu$s) were observed for the reaction of LDAO solubilized *R. sphaeroides* RCs with *R. capsulatus* cyt $c_2$ at low ionic strength, in the relative proportions of 9 to 1 with an apparent $K_D$ of 4−6 $\mu$M for both sites. Moreover, depending on the species of cyt used, the relative proportions of the two high-affinity sites varied considerably (from a single site to roughly equal amounts of two high-affinity sites). Drepper et al. (*8*) studied electron-transfer kinetics from cyt $c_2$ to LDAO-solubilized *R. sphaeroides* RCs using zero-length cross-linking between the cyt and the RC and found two first-order processes. They concluded that the two kinetic phases involve the same exclusive site for binding cyt $c_2$, but with two complexes of different geometry. Overfield and Wraight (*7*) reported two binding sites for reduced horse cyt *c* using LDAO-solubilized RCs, one photochemically active ($K_D \sim 1$ $\mu$M) and one photochemically inactive ($K_D < 10$ nM) at low ionic strength. Thus, our observation of two reduced cyt binding sites is not unprecedented (see below for further discussion). A key question that we cannot address directly under the conditions of the PWR experiment is whether both of the binding sites for reduced wild-type cyt $c_2$ that we observe are photochemically active. On the basis of studies cited above, the two sites we observe could be photochemically active, and we will assume so for the subsequent discussion.

At 109 mM ionic strength, we find that the $K_D$ values actually decrease (i.e., affinities increase) relative to 19 mM with the wild-type reduced cyt, ~5-fold for the high-affinity site, ~2-fold for the low-affinity site for wild-type, and ~2-fold for reduced K93P (Table 1). This is contrary to the expectation based on kinetic studies where a strong effect of ionic strength is observed (LDAO-solubilized RCs), with $k_{on}$ (eq 1) decreasing ~10-fold between 19 and 109 mM ionic strength [although not measuring precisely the same reaction, $RC^+ + c_2(Fe^{2+})$ versus $RC + c_2(Fe^{2+})$] (34). The ionic strength effect on $k_{on}$ is consistent with a decrease in affinity at high ionic strength (assuming $k_{off}$ does not change with ionic strength). Note that LDAO has a positive charge and may affect electrostatics in such a way as to mask or partially mask the effect of ionic strength on the kinetic measurements. However, the effect of ionic strength on the binding of cyt ($c_2$ or *c*) to RCs incorporated in phospholipid vesicles (*3*, *35*) and steady-state turnover of photooxidized RCs (*5*) are consistent with a substantial decrease in affinity as the ionic strength is increased. Thus, our finding that $K_D$ decreases with increasing ionic strength is not consistent with the studies cited above. However, the conditions used here (solid-supported planar bilayer) are substantially different than in the previous studies (detergent-solubilized RCs or unilameller vesicles in the presence of detergent, and horse cyt *c* in some cases). Further studies will be required to understand the differences in the effect of ionic strength reported here.

The decrease in $K_D$ at high ionic strength reported here suggests that nonpolar interactions play an important role in binding. As the ionic strength is increased, $k_{on}$ decreases, presumably because of the key role that electrostatics play in recognition and formation of the cyt−RC encounter complex, but nonpolar interactions, important in the release of the cyt (either redox state in the case of the wild-type cyt), are enhanced. This could result in a net increase in affinity depending on the relative effects of ionic strength on the on and off rate constants. This interpretation is consistent with the recent work of Gong et al. (*11*), who find that interfacial hydrophobic side chains play a key role in controlling both $k_{ET}$ and $K_D$, which they find are strongly correlated with the affinity increasing with increasing $k_{ET}$.

A significant advantage of PWR is the ability to measure changes in mass and structural anisotropy on binding.

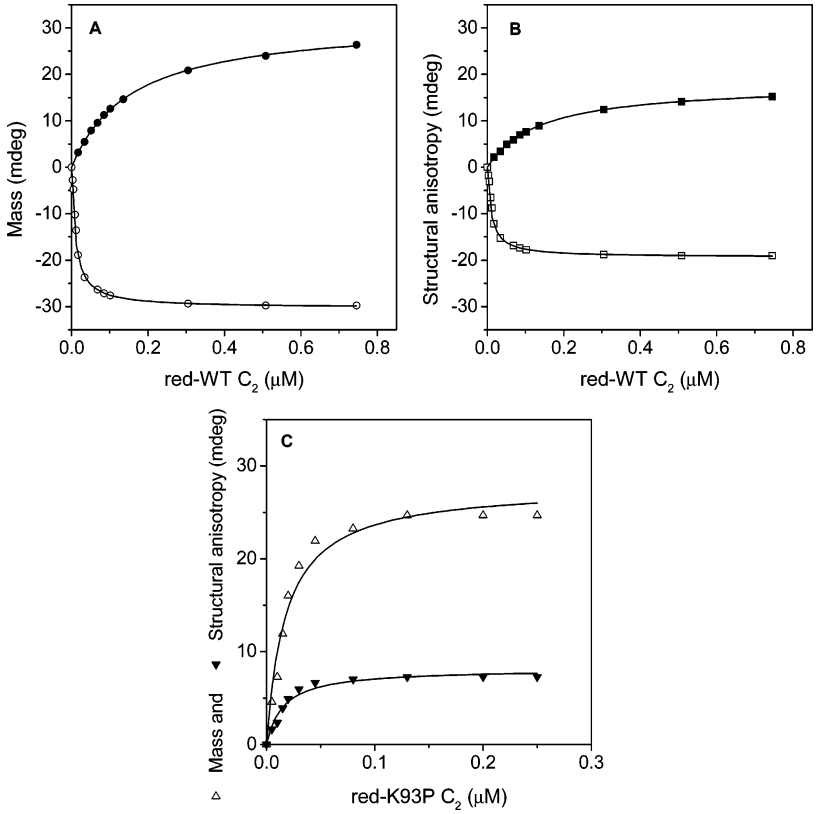


FIGURE 5: Mass and structural anisotropy changes as a function of reduced cyt $c_2$ concentration at 109 mM ionic strength. Data points for mass and structural anisotropy changes are calculated using the plots shown in Figure 4. The solid lines through the data points are fits using a single hyperbolic function with the dissociation constants as given in Table 1. (A) Mass changes obtained for the high-affinity (○) and low-affinity (●) binding processes for reduced wild-type cyt $c_2$. (B) Structural anisotropy changes obtained for the high-affinity (■) and low-affinity (□) binding processes for reduced wild-type cyt $c_2$. (C) Mass (△) and structural anisotropy (▼) changes for binding of reduced K93P mutant.

Table 2: Deconvolution of Mass and Structural Anisotropy (SA) Changes for Cyt $c_2$ Binding to RCs

| | contribution of mass and structural anisotropy to PWR | | | |
|---|---|---|---|---|
| | oxidized cyt | | reduced cyt | |
| cytochrome | mass (%) | mass/SA | mass (%) | mass/SA |
| Ionic Strength = 109 mM | | | | |
| wild-type | 81.4 ± 2.0 | 4.6 | 72.0 ± 0.1/75.0 ± 1.5[a] | 2.6/3.0[a] |
| K93P | 79.0 ± 2.6 | 3.8 | 77.0 ± 1.5 | 3.3 |
| Ionic Strength = 19 mM | | | | |
| wild-type | 72.5 ± 0.2 | 2.6 | 66.5 ± 1.1/62.3 ± 2.3[a] | 2.0/1.7[a] |
| K93P | 69.4 ± 0.8 | 2.3 | 69.0 ± 0.7 | 2.2 |

[a] High-affinity site/low-affinity site.

Clearly, the two binding sites observed with reduced wild-type cyt $c_2$ have very different properties, with binding to the high-affinity site resulting in a decrease in both mass and structural anisotropy. This result requires that binding at the high-affinity site causes the RC to contract along the normal and move the protein mass further into the membrane, thereby expelling phospholipids and resulting in a net decrease in membrane mass and in structural anisotropy (i.e., the axial ratio of the RC decreases). Binding to the second site reverses the mass and anisotropy loss. However, it is interesting that the proportions of the mass vs structural changes are approximately the same for the two sites (72 and 75% mass contribution, Table 2) but with opposite effects.

There are three possibilities to explain the wild-type cyt $c_2$ binding data. First, a separate site model in which there are two independent sites on the RC with substantially different affinities, one driving a structural change, which results in decreasing mass and structural anisotropy, and the other increasing mass and structural anisotropy. This model is consistent with the data in that two clearly distinct hyperbolic processes are observed which, on the basis of the magnitudes of the PWR signal changes, appear to be about equal in occupancy (comparing amplitudes of curves 1 vs 2 and 3 vs 4 in Figure 2A,B). A second possibility is that the binding of a cyt to the low-affinity site drives a structural change that results in the release of the cyt bound to the high-affinity site (that is, results in a large decrease in affinity). This model would result in reversing the decrease in mass and in structural anisotropy as observed. These two alternatives cannot be distinguished at the present time. The third possibility is that there are two populations of RCs (or conformers of reduced cyt $c_2$) present with distinct affinities and at approximately equal concentrations. This is less likely

than the previous possibilities, although it cannot be ruled out by these data (however, see below).

Oxidized wild-type cyt $c_2$ binds to a single site with a positive shift in the PWR spectra, which is consistent with an increase in mass and increased anisotropy, as does the low-affinity reduced site. As can be seen in Table 2, the percentage of the shift due to mass change is larger for the oxidized than for reduced cyt at both ionic strengths with wild-type cyt. Note that both redox states of the K93P mutant also have a positive increase in the PWR signal on binding at a single site. Again, the structural change accounts for a smaller proportion of the shift than the mass change (Table 2). These observations appear to exclude multiple RC populations as an explanation for the two sites available for reduced wild-type cyt. Moreover, the existence of two conformers of reduced wild-type cyt $c_2$ also seems unlikely, since the reduced cyt $c_2$ has substantially greater stability relative to the oxidized state, suggesting that if multiple cyt $c_2$ conformers exist, they would be seen in the oxidized not reduced form of cyt $c_2$. The common factors between oxidized wild-type cyt $c_2$ and both redox states of K93P, which correlates with a single hyperbolic curve, is that they show an increase in mass and anisotropy on RC binding and are all significantly less stable to denaturation than is reduced wild-type. On the basis of these observations, the results are consistent with a model in which there are two independent binding sites on the RC surface, with the high-affinity site requiring a cyt $c_2$ conformer that can only be accessed by the reduced wild-type cyt, whereas the low-affinity site is accessible to the reduced wild-type and the less stable (more dynamic) oxidized form or less stable reduced forms (i.e., reduced K93P). This interpretation will be tested in future studies. It follows then that binding to the high-affinity site drives a structural change, which moves the RC into the membrane, resulting in a loss of mass by displacement of lipid, while the low-affinity site positions the bound cyt further away from the membrane, increasing the apparent mass and the anisotropy. Thus, for purposes of comparison, we equate the low-affinity reduced site and the oxidized site, which have similar but not identical behavior in terms of the effect of binding on mass and structural anisotropy. Note also that the effect of increasing ionic strength is to significantly increase the contribution of the mass change (decrease the contribution of structural change) to the PWR spectral shifts (Table 2), which is true for both wild-type and the mutant and for both redox states.

As discussed above in the case of binding of reduced cyt (wild-type and K93P), there is a small increase in affinity on increasing the ionic strength from 19 to 109 mM (2−5-fold). However, wild-type oxidized cyt has a ∼30-fold stronger affinity at high ionic strength. The net result, equating the low-affinity site for reduced wild-type and the oxidized wild-type binding site based on the directions of the spectral shifts, and hence the nature of the induced conformational change, is differential binding of the two wild-type redox states at high ionic strength ($K_D$ = 10 nM for oxidized vs 150 nM for reduced). In the case of K93P, there is also differential binding at high ionic strength, but in this case, the reduced form is more tightly bound ($K_D$ = 24 vs 310 nM for oxidized). Assuming that the ∼20-fold increase in the hinge movement in the K93P mutant compared to wild-type cyt facilitates the release of the oxidized state from the RC−cyt complex, then a large increase in $K_D$ would be expected and was observed (310 nM for K93P vs 10 nM for wild-type, at 109 mM ionic strength). Thus, the results presented here suggest that hinge dynamics play a role in electron transfer under physiological conditions by driving the dissociation of the oxidized cyt. This would facilitate the entrance of a second electron into the RC as required for full quinone reduction.

Interestingly, comparing the low-affinity reduced wild-type site and reduced K93P binding, the affinity for reduced K93P is ∼6-fold greater than for reduced wild-type at both ionic strengths studied. This could be attributed to the replacement of lysine by a more hydrophobic proline, which results in a substantially decreased $k_{off}$, hence a higher apparent affinity. The situation with binding of oxidized wild-type as compared to oxidized K93P is less clear. Assuming, that, at high ionic strength, hinge dynamics are dominant in the case of K93P, we can rationalize the 31-fold decrease in affinity for oxidized K93P relative to wild-type. However, at 19 mM ionic strength, the affinity of the oxidized K93P is ∼2-fold greater than that for wild-type, suggesting that the hinge dynamics do not play a role in binding at this ionic strength, although it is not clear what is responsible for the difference in $K_D$ values. Unfortunately, hinge dynamics have been measured only at high ionic strength, necessitated by the use of high concentrations of imidazole to determine the rate constants (*25*). Hence, it remains to be seen if oxidized K93P hinge dynamics are altered at low ionic strength.

In summary, although much more needs to be done to fully understand the apparent affinity of RCs for cyt $c_2$ as determined by PWR, nevertheless, a number of points are clear. First, PWR provides high-quality binding and conformational data under conditions that closely resemble the physiological situation (high ionic strength, RC incorporated into a phospholipid bilayer). Second, there are two binding sites for reduced wild-type cyt $c_2$ (independent of ionic strength) with only one of these sites available to the oxidized wild-type cyt. Third, combining the binding data for oxidized wild-type cyt $c_2$ and the K93P mutant (both redox states), it can be suggested that the second, high-affinity site requires a more stable conformation than the low affinity site. Fourth, we find that nonpolar interactions appear to play an important role in the affinity of RCs for cyt $c_2$, a result not inconsistent with recent kinetic studies (*11*). Fifth, using a cyt $c_2$ mutant (K93P) with substantially altered hinge dynamics, we have evidence that hinge dynamics facilitate the dissociation of oxidized cyt from the transient cyt $c_2$−RC complex at high ionic strength.

## REFERENCES

1. Dutton, P. L., Petty, K. M., Bonner, H. S., and Morse, S. D. (1975) Cytochrome $c_2$ and reaction center of *Rhodopseudomonas sphaeroides* Ga. membranes. Extinction coefficients, content, half-reduction potentials, kinetics and electric field alterations, *Biochim. Biophys. Acta 387*, 536−556.
2. Rosen, D., Okamura, M. Y., and Feher, G. (1980) Interaction of cytochrome *c* with reaction centers of *Rhodopseudomonas sphaeroides* R-26: determination of number of binding sites and dissociation constants by equilibrium dialysis, *Biochemistry 19*, 5687−5692.
3. Pachence, J. M., Dutton, P. L., and Blasie, J. K. (1983) A structural investigation of cytochrome *c* binding to photosynthetic reaction centers in reconstituted membranes, *Biochim Biophys Acta 724*, 6−19.

4. Tiede, D. M., Vashishta, A. C., and Gunner, M. R. (1993) Electron-transfer kinetics and electrostatic properties of the *Rhodobacter sphaeroides* reaction center and soluble c-cytochromes, *Biochemistry 32*, 4515−4531.
5. Gerencser, L., Laczko G., and Marti, P. (1999) Unbinding of oxidized cytochrome *c* from photosynthetic reaction center of *Rhodobacter sphaeroides* is the bottleneck of fast turnover, *Biochemistry 38*, 16866−71685.
6. Tetreault, M., Rongey, S. H., Feher, G., and Okamura, M. Y. (2001) Interaction between cytochrome $c_2$ and the photosynthetic reaction center from *Rhodobacter sphaeroides*: effects of charge-modifying mutations on binding and electron transfer, *Biochemistry 40*, 8452−8462.
7. Overfield, R. E., and Wraight, C. A. (1986) Photooxidation of mitochondrial cytochrome *c* by isolated bacterial reaction centers: Evidence for tight-binding and diffusional pathways, *Photosyn. Res. 9*, 167−179.
8. Drepper, F., Dorlet, P., and Mathis, P. (1997) Cross-linked electron-transfer complex between cytochrome $c_2$ and the photosynthetic reaction center of *Rhodobacter sphaeroides*, *Biochemistry 36*, 1418−1427.
9. Tiede, D. M., and Dutton, P. L. (1993) Electron Transfer between Bacterial Reaction Centers and Mobile c-Type Cytochromes, In *The Photosynthetic Reaction Center* (Deisenhofer, J.; Norris J. R., Eds.) Vol. 1, pp 257−88, Academic Press, San Diego, CA.
10. Tetreault, M., Cusanovich, M. A., Meyer, T. E., Axelrod, H., and Okamura, M. Y. (2002) Double mutant studies identify electrostatic interactions that are important for docking cytochrome $c_2$ onto the bacterial reaction center, *Biochemistry 41*, 5807−5815.
11. Gong, X. M., Paddock, M. L., and Okamura, M. Y. (2003) Interactions between cytochrome $c_2$ and photosynthetic reaction center from *Rhodobacter sphaeroides*: Changes in binding affinity and electron transfer rate due to mutation of interfacial hydrophobic residues are strongly correlated, *Biochemistry 42*, 14492−14500.
12. Berghuis, A. M., and Brayer, G. D. (1992) Oxidation State-dependent Conformational Changes in Cytochrome *c*, *J. Mol. Biol. 223*, 959−976.
13. Sogabe, S., and Miki, K. (2001) Crystal structure of the oxidized cytochrome $c_2$ from *Blastochloris viridis*, *FEBS Lett. 491*, 174−179.
14. Lett, C. M. Berghuis, A. M., Frey, H. E., and Guillemette, J. G. (1996) The role of a conserved water molecule in the redox-dependent thermal stability of iso-1-cytochrome *c*, *J. Biol. Chem. 271*, 29088−29093.
15. Banci, L., Bertini, I., Gray, H. B., Luchinat, C., Reddig, T., Rosato, A., and Turano, P. (1997) Solution Structure of Oxidized Horse Heart Cytochrome *c*, *Biochemistry 36*, 9867−9877.
16. Banci, L, Bertini, I., Huber, J. G., Spyroulias, G. A., and Turano, P. (1999) Solution structure of reduced horse cytochrome *c*, *J. Biol. Inorg. Chem. 4*, 21−31.
17. Berghuis, A. M., Guillemette, J. G., McLendon, G., Sherman, F., Smith, M., and Brayer, G. D. (1994) The role of a conserved internal water molecule and its associated hydrogen bond network in cytochrome *c*, *J. Mol. Biol. 36*, 786−799.
18. Moser, C. C., and Dutton, P. L. (1988) Cytochrome *c* and $c_2$ Binding Dynamics and Electron Transfer with Photosynthetic Reaction Center Protein and Other Integral Membrane Redox Proteins, *Biochemistry 27*, 2450−2461.
19. Larson, J. W., and Wraight, C. A. (2000) Preferential Binding of Equine Ferricytochrome *c* to the Bacterial Photosynthetic Reaction Center from *Rhodobacter sphaeroides*, *Biochemistry 39*, 14822−14830.
20. Dumortier, C., Holt, J. M., Meyer, T. E., and Cusanovich, M. A. (1998) Imidazole Binding to *Rhodobacter capsulatus* Cytochrome $c_2$. Effect of Site-Directed Mutants on Ligand Binding, *J. Biol. Chem. 273*, 25647−25653.
21. Schejter, A., and Aviram, I. (1969) The reaction of cytochrome *c* with imidazole, *Biochemistry 8*, 149−153.
22. Sutin, N., and Yandell, J. K. (1972) Mechanisms of the reactions of cytochrome *c*. Rate and equilibrium constants for ligand binding to horse heart ferricytochrome *c*, *J. Biol. Chem. 247* (21), 6932−6936.
23. Axelrod, H. L., Feher, G., Allen, J. P., Chirino, A. J., Day, M. W., Hsu, B. T., and Rees, D. C. (1994) Crystallization and X-ray structure determination of cytochrome $c_2$ from *Rhodobacter sphaeroides* in three crystal forms, *Acta Crystallogr. D50*, 596−602.
24. Banci, L, Bertini, I., Liu, G., Lu, J., Reddig, T., Tang, W., Wu, Y., Yao, Y., and Zhu, D. (2001) Effects of extrinsic imidazole ligation on the molecular and electronic structure of cytochrome *c*, *J. Biol. Inorg. Chem. 6*, 628−637.
25. Dumortier, C., Remaut, H., Fitch, J., Meyer, T. E., Van Beeumen, J., and Cusanovich, M. A. (2004) Protein dynamics in the region of the sixth ligand methionine revealed by studies of imidazole binding to *Rhodobacter capsulatus* cytochrome $c_2$ hinge mutants, *Biochemistry 43*, 7717−7724.
26. Salamon, Z., and Tollin, G. (2001) Optical anisotropy in lipid bilayer membranes: coupled plasmon-waveguide resonance measurements of molecular orientation, polarizability, and shape, *Biophys. J. 80*, 1557−1567.
27. Salamon, Z., and Tollin, G. (2001) Plasmon resonance spectroscopy: probing molecular interactions at surfaces and interfaces, *Spectroscopy 15*, 161−175.
28. Salamon, Z., and Tollin, G. (2004) Graphical analysis of mass and anisotropy changes observed by plasmon-waveguide resonance spectroscopy can provide useful insights into membrane protein function, *Biophys. J. 86*, 2508−2516.
29. Salamon, Z., Macleod, H. A., and Tollin, G. (1997) Coupled plasmon-waveguide resonators: a new spectroscopic tool for probing proteolipid film structure and properties, *Biophys. J. 73*, 2791−2797.
30. Salamon, Z., Wang, Y., Tollin, G., and Macleod, H. A. (1994) Assembly and molecular organization of self-assembled lipid bilayers on solid substrates monitored by surface plasmon resonance spectroscopy, *Biochim. Biophys. Acta 1195*, 267−275.
31. Marinetti, G. V., and Cattieu, K. (1981) Lipid analysis of cells and chromatophores of *Rhodopseudomonas sphaeroides*, *Chem. Phys. Lipids 28*, 241−251.
32. Salamon, Z., and Tollin, G. (1999) *Surface plasmon resonance. I. Theoretical Principles, Encyclopedia of Spectroscopy and Spectrometry* (Lindon, J. C., Tranter, G. E., and Holmes, J. L., Eds.) Vol. 3, pp 2311−2319, Academic Press, New York.
33. Imhoff, J. F., Kushner, D. J., Kushwaha, S. C., and Kates, M. (1982) Polar lipids in phototrophic bacteria of the Rhodospirillaceae and Chromatiaceae families, *J. Bacteriol. 150*, 1192−1201.
34. Caffrey, M. S., Bartsch R. G., and Cusanovich, M. A. (1992) Study of the cytochrome $c_2$-reaction center interaction by site-directed mutagenesis, *J. Biol. Chem. 267*, 6317−6321.
35. Overfield, R. E., and Wraight, C. A. (1980) Oxidation of Cytochromes *c* and $c_2$ by Bacterial Photosynthetic Reaction Centers in Phospholipid Vesicles. 1. Studies with Neutral Membranes, *Biochemistry 19*, 3322−3327.


BI0481904